Coarse-grained *NN* potential with chiral two-pion exchange

R. Navarro Pérez,* J. E. Amaro,† and E. Ruiz Arriola‡
Departamento de Física Atómica, Molecular y Nuclear, and Instituto Carlos I de Física Teórica y Computacional, Universidad de Granada, E-18071 Granada, Spain

(Received 6 November 2013; revised manuscript received 20 December 2013; published 26 February 2014)

We determine the chiral constants of the nucleon-nucleon two-pion exchange potential deduced from chiral perturbation theory. By using a coarse-grained representation of the short-distance interactions with 30 parameters, the partial wave analysis fit gives $\chi^2/\nu = 1.07$ to a mutually consistent set of 6713 data previously built from all proton-proton and neutron-proton scattering data published from 1950 to 2013 with laboratory energies below 350 MeV. We obtain $(c_1,c_3,c_4) = (-0.41 \pm 1.08, -4.66 \pm 0.60, 4.31 \pm 0.17)$ GeV^{-1} with an almost 100% anticorrelation between c_1 and c_3. We also provide the errors in the short-distance parameters and propagate them to the deuteron properties and low partial wave phase shifts.

DOI: 10.1103/PhysRevC.89.024004 PACS number(s): 03.65.Nk, 11.10.Gh, 13.75.Cs, 21.30.Fe

I. INTRODUCTION

The modern chiral theory of the nuclear forces era started in 1990 when Weinberg suggested [1] using effective field theory in conjunction with chiral symmetry to derive in a systematic and model-independent way the forces between many nucleons complying with the symmetries of quantum chromodynamics (QCD). The chiral perturbation theory (ChPT) predicts an increasing suppression of n-body forces at long distances and hence was further elaborated [2] and applied to *NN* data soon thereafter [3]. This requires the introduction of counterterms encoding the *unknown* short distance piece of the interaction and which are not directly constrained by chiral symmetry (see, e.g., [4,5] for reviews).

While one-pion exchange (OPE) is a quite universal feature of most phenomenological *NN* interactions and a simple consequence of the meson exchange picture, chiral two-pion exchange (χTPE) arises as a consequence of the spontaneous breakdown of chiral symmetry; and the chiral constants c_1,c_3, and c_4 appearing in πN scattering at low energies emerge at the next-to-next-to-leading order (N2LO) in the chiral expansion of the *NN* force [6]. Because the *NN* interaction is a basic building block in nuclear physics, the consistency of both determinations is a necessary and important condition for the verification of this upgraded view of nuclear physics. A comparative overview of different πN and *NN* determinations up to 2005 is presented in Ref. [7].

Our purpose is to extract c_1, c_3, and c_4 from a partial wave analysis (PWA) of the 8124 published proton-proton and neutron-proton scattering data collected from 1950 till 2013 and using the *NN* chiral potential up to N2LO in the Weinberg counting [6]. We stress that we are *not* making a ChPT calculation which would only apply below laboratory (LAB) energies sensing the 3π-exchange left cut, $E_{\rm LAB} = (2/M_N)(3m_\pi/2)^2 \lesssim 100$ MeV. We rather determine the long-distance tail of the potential constraining the short-distance interaction with higher energies. We recall that according to well-known statistical principles, it is essential to validate the fit to the data with a χ^2 per degree of freedom $\chi^2/\nu \sim 1$ with $\nu = N_{\rm Data} - N_{\rm par}$ before errors in fitting parameters can be determined.

Much of the present understanding of *NN* interactions has profited immensely from the long-term in-depth studies of the Nijmegen group, which culminated with the concept of high quality interactions, i.e., with $\chi^2/\nu \sim 1$ [8,9]. Subsequent analyses have been built upon these works by incorporating new data and potential forms [10–12] including the chiral TPE analysis of the Nijmegen group [13,14]. In our most recent work [15,16] a refined rejection criterion was applied and a large number of data published since the original Nijmegen PWA below the pion production threshold [8,9] have been added to the database, almost doubling the total number. The present work represents an upgrade of the chiral TPE-PWA [13,14] with this new data set keeping identical the long-range part of the interaction, in particular the OPE and TPE part as well as the electromagnetic effects, but using the computationally convenient δ-shell representation [15,16] for the unknown short-range contribution to the *NN* potential.

The paper is organized as follows. In Sec. II we describe the main new issues considered in our analysis. Details of the fit involving χTPE are discussed in Sec. III. After that, in Sec. IV, we discuss the error analysis of our fits. Using the covariance matrix obtained from our analysis of the data, we are in a position to propagate uncertainties and list np and pp phases with statistical errors based on χTPE potentials in Sec. V. Finally, in Sec. VI we come to our main conclusions.

II. *NN* DATA AND COARSE-GRAINED POTENTIALS

The large body of published data is not fully consistent, as recognized by earlier high quality fits [8–12], i.e., having $\chi^2/\nu \lesssim 1$. The problem was handled by using a rejection criterion at the 3σ confidence level. In Refs. [15,16] we use a procedure suggested by Gross and Stadler [12] which essentially provides a self-consistent way of analyzing the tension among all the data and 3σ-rejecting mutually inconsistent data. This is done by using a charge-dependent OPE potential plus

*rnavarrop@ugr.es
†amaro@ugr.es
‡earriola@ugr.es

TABLE I. Complete *NN* database from PWA without rejection. $N_{\rm Data} = 8124$.

r_c (fm)	1.8		2.4		3.0	
	$N_{\rm p}$	χ^2/ν	$N_{\rm p}$	χ^2/ν	$N_{\rm p}$	χ^2/ν
OPE	31	1.80	39	1.56	46	1.54
TPE(NLO)	31	1.72	38	1.56	46	1.52
TPE(N2LO)	30+3	1.60	38+3	1.56	46+3	1.52

TABLE III. Consistent *NN* database from the improved 3σ criterion. $N_{\rm Data} = N_{\rm accept}^{({\rm OPE},r_c=3{\rm fm})} = 6713$.

r_c (fm)	1.8		2.4		3.0	
	$N_{\rm par}$	χ^2/ν	$N_{\rm par}$	χ^2/ν	$N_{\rm par}$	χ^2/ν
OPE	31	1.38	39	1.09	46	1.04
TPE(NLO)	31	1.24	38	1.07	46	1.05
TPE(NNLO)	30+3	1.07	38+3	1.07	46+3	1.05

electromagnetic effects such as vacuum polarization, magnetic moments interaction, etc., above a cutoff radius of $r_c = 3$ fm (see Ref. [16] for a recollection of the formulas). The short-range part is most conveniently parametrized following Aviles [17] as a sum of Dirac δ shells located at equidistant points below r_c and separated by $\Delta r = 0.6$ fm (see also [18–22] for further details and applications). The short-range *NN* interaction can be written as a sum of δ shells, so that the total potential reads

$$V(r) = \sum_{n=1}^{21} O_n \left[\sum_{i=1}^{N} V_{i,n} \Delta r_i \delta(r - r_i) \right] + V_{\rm long}(r)\theta(r - r_c), \quad (1)$$

where O_n are the set of operators in the AV18 basis [10], $r_i \leqslant r_c$ are a discrete set of N radii, $\Delta r_i = r_{i+1} - r_i$, and $V_{i,n}$ are unknown coefficients to be determined from data. The $r > r_c$ piece, $V_{\rm long}(r)$ contains a charge-dependent (CD) one-pion exchange (OPE) and electromagnetic (EM) corrections which are kept fixed throughout:

$$V_{\rm long}(r) = V_{\rm OPE}(r) + V_{\rm EM}(r)\,. \quad (2)$$

The form of the complete potential includes an operator basis extending the AV18 potential [10] and specified in Refs. [15,16] but the statistical analysis is carried out more effectively in terms of some low and independent partial wave contributions to the potential from which all other higher partial waves are consistently deduced (see Refs. [15,16]). The PWA allows one to accept $N_{\rm accept} = 6713$ data with a $\chi^2/\nu = 1.04$. The present work uses this fixed database which is extensively described in Refs. [15,16], and the *same* long-range potentials.

III. FIT OF TWO-PION EXCHANGE POTENTIAL

In this work we keep the OPE piece with the recommended value $f^2 = 0.075$ [23,24] as we did in Refs. [15,16] and add the χTPE potential [6] to the long-range piece,

$$V_{\rm long}(r) = V_{\chi{\rm TPE}}(r) + V_{\rm OPE}(r) + V_{\rm EM}(r)\,. \quad (3)$$

We also modify the cutoff radius r_c to be determined from a fit to the data. Namely, we take the values $r_c = 3$, 2.4, and 1.8 fm. This reduces the number of δ shells and hence the number of short-distance parameters $\lambda_{i,n}$. The three chiral constants c_1, c_3, and c_4 of the χTPE potential will be additional parameters of the fit. Since we aim at a determination of uncertainties in these parameters we can only do so provided the fit is acceptable, i.e., $\chi^2/\nu \sim 1$. The quality of our fits regarding the influence of TPE in the description of the data can be judged by analyzing three different schemes which are displayed in Tables I–III.

In Table I we show the χ^2 values corresponding to a direct fit to all the data without rejecting any of the published experimental results gathered from 1950 until 2013. As we see, the large χ^2 values correspond to an unacceptable fit and hence prevent error determination and propagation. In Table II we show the χ^2 values corresponding to a dynamical database fit to all the data subjected to the 3σ criterion [8–12], so that the selection of the data depends on the description of the long-range interaction, which in our case is χTPE, and on the value of the cutoff radius r_c. As we see, there is a reduction on

TABLE II. 3σ-selected *NN* database from potential analysis.

r_c (fm)	1.8			2.4			3.0		
	$N_{\rm accept}$	$N_{\rm par}$	χ^2/ν	$N_{\rm accept}$	$N_{\rm par}$	χ^2/ν	$N_{\rm accept}$	$N_{\rm par}$	χ^2/ν
OPE	5766	31	1.10	6363	39	1.09	6438	46	1.06
TPE(NLO)	5841	31	1.10	6432	38	1.10	6423	46	1.06
TPE(N2LO)	6220	30+3	1.07	6439	38+3	1.10	6422	46+3	1.06

TABLE IV. χ^2 values for different analyses up to $E_{\rm LAB} \leqslant 350$ MeV, PWA93 [8], Nijm I [9], Nijm II [9], Reid93 [9], AV18 [10], CD-Bonn [11], WJC1 and WJC2 [12], PWA pp-TPE [13], and PWA NN-TPE [14] (* means fit up to $E_{\rm LAB} \leqslant 500$ MeV), δ-OPE [15], and δ-TPE (present work). N_{pp} (N_{np}) denotes the number of pp (np) data, $N_{\rm Dat} = N_{pp} + N_{np}$ is the total number of fitted data, $N_{\rm Par}$ is the number of parameters and χ^2/ν the corresponding χ^2 per degree of freedom $\nu = N_{\rm Dat} - N_{\rm Par}$.

Potential	N_{pp}	χ^2_{pp}	N_{np}	χ^2_{np}	$N_{\rm Dat}$	$N_{\rm Par}$	χ^2/ν
PWA93	1787	1787	2526	2489	4313	39	1.01
NijmI	1787	1795	2526	2627	4313	41	1.03
NijmII	1787	1795	2526	2625	4313	47	1.03
Reid93	1787	1795	2526	2694	4313	50	1.03
Nijm93	1787	3175	2526	4848	4313	15	1.87
AV18	1787	1962	2526	2685	4313	40	1.09
CDBonn	2932	2153	3058	3119	5990	43	1.02
WJC1	0		3788	4015	3788	27	1.06
WJC2	0		3788	4015	3788	15	1.12
ppχTPE	1951	1937	0		1951	25	1.01
NNχTPE*	5109	5184	4786	4806	9895	73	1.02
δ-OPE	2996	3051	3717	3958	6711	46	1.04
δ-χTPE	2996	3177	3716	4058	6711	33	1.08

TABLE V. Fitting δ-shell partial wave parameters $(\lambda_n)^{JS}_{l,l'}$ (in fm^{-1}) with their errors for all states in the JS channel. We take $N = 3$ equidistant points with $\Delta r = 0.6$ fm. The dash indicates that the corresponding fitting $(\lambda_n)^{JS}_{l,l'} = 0$. In the first line we provide the central component of the δ shells corresponding to the EM effects below $r_c = 1.8$ fm. These parameters remain fixed within the fitting process.

Wave $V_C[pp]_{\rm EM}$	λ_1 ($r_1 = 0.6$ fm) 0.02069940	λ_2 ($r_2 = 1.2$ fm) 0.01871309	λ_3 ($r_3 = 1.8$ fm) 0.00460163
$^1S_0[np]$	1.48(7)	−0.86(1)	−0.041(7)
$^1S_0[pp]$	1.87(3)	−0.875(5)	−0.045(3)
$^3P_0$	2.318(3)	0.400(7)	−0.093(3)
$^1P_1$	–	1.09(1)	–
$^3P_1$	–	1.27(1)	0.008(3)
$^3S_1$	1.16(2)	–	−0.073(4)
ε_1	–	−2.50(2)	−0.097(4)
$^3D_1$	–	2.03(6)	–
$^1D_2$	–	−0.494(9)	−0.034(4)
$^3D_2$	–	−0.82(1)	−0.148(5)
$^3P_2$	−0.953(4)	−0.233(4)	−0.034(2)
ε_2	–	0.85(2)	0.042(2)
$^3F_2$	–	4.05(9)	−0.110(4)
$^1F_3$	–	1.7(1)	–
$^3D_3$	–	0.73(1)	–

the χ^2 value but the number of rejected data differ among each other. The data rejection triggered by the χTPE potential does not correspond to eliminate mutually inconsistent data, but rather to shape the database to better comply to the chiral theory, and in our view represents a bias which definitely induces a systematic error in the analysis. Finally, in Table III we use the fixed and consistent data from the OPE $r_c = 3$ fm analysis based on the improved 3σ criterion of Gross and Stadler [12] carried out in practice in our recent work [21]. In this case, an acceptable $\chi^2/\nu = 1.07$ with 30 parameters allows us to determine and propagate errors.

A comprehensive overview of several high quality analyses up to $E_{\rm LAB} \leqslant 350$ MeV is presented in Table IV. This includes PWA93 [8], Nijm I [9], Nijm II [9], Reid93 [9], AV18 [10], CD-Bonn [11], WJC1 and WJC2 [12], PWA pp-TPE [13], and PWA NN-TPE [14] (here $E_{\rm LAB} \leqslant 500$ MeV) as well as our recent δ-shell-OPE fit [15]. As one sees, the quality of the fit depends on both the number of parameters as well as the total number of analyzed data.

TABLE VI. Summary of chiral constants c_1, c_3, and c_4 (in GeV^{-1}) compared with determinations. The symbol * stands for input from πN.

	Ref.	Source	c_1	c_3	c_4
This work		*NN*	−0.41(1.08)	−4.66(60)	4.31(17)
Nijmegen	[13]	*pp*	−0.76(07)*	−5.08(28)	4.70(70)
Nijmegen	[14]	*NN*	−0.76(07)*	−4.88(10)	3.92(22)
E & M a	[32]	*NN*	−0.81	−3.40	3.40
E & M b	[32]	*NN*	−0.81	−3.20	5.40
PV & RA	[31]	*NN*	−1.2(2)	−2.6(1)	3.3(1)
Ekström *et al.*	[29]	*NN*	−0.92	−3.89	4.31
B & M	[33]	πN	−0.81(15)	−4.69(1.34)	3.40(4)

IV. ERROR ANALYSIS WITH TPE POTENTIAL

As already mentioned, the inclusion of the χTPE potential [6] allows us to describe the interaction in the region below 3 fm and reduces the cutoff radius down to $r_c = 1.8$ fm, before sensing nucleon finite size effects (see, e.g., the discussion in Ref. [22]). Thus, some of the δ shells which generally coarse grain the interaction are removed in favor of an underlying and explicit chiral representation. As in our previous PWA using OPE [15,16] we impose the *np* and *pp* contributions to be identical in all isovector partial waves except the $^1S_0$. This yields $\chi^2/\nu = 1.08$, a slightly higher value than with our OPE PWA, but improving over the much used AV18 potential where $\chi^2/\nu = 1.09$ [10] and where the number of data was about 60% less than in the present analysis. The most recent study was based on the covariant spectator model [12] where only *np* was considered (see Table IV).

The resulting short-distance parameters and their errors are presented in Table V. The first line corresponds to a coarse graining of the *known* electromagnetic part of the interaction as described in Refs. [15,16] and, like there, these parameters are fixed throughout the fitting process. As we see only the innermost λ_1 significantly differs by 25% in the *np* and *pp* $^1S_0$ waves.

While this isospin violation prevents in our view a sensible prediction for the *nn* $^1S_0$ scattering length based solely on

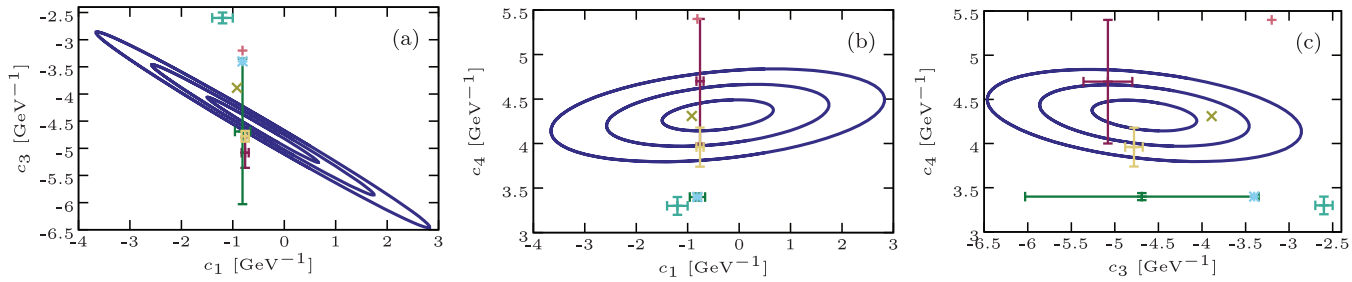

FIG. 1. (Color online) Correlation ellipses for the chiral constants c_1, c_3, and c_4 appearing in the TPE potential with a cutoff radius of $r_c = 1.8$ fm from a PWA with the consistent database and with $\chi^2/\nu = 1.1$. The crosses represent the various determinations listed in Table VI.

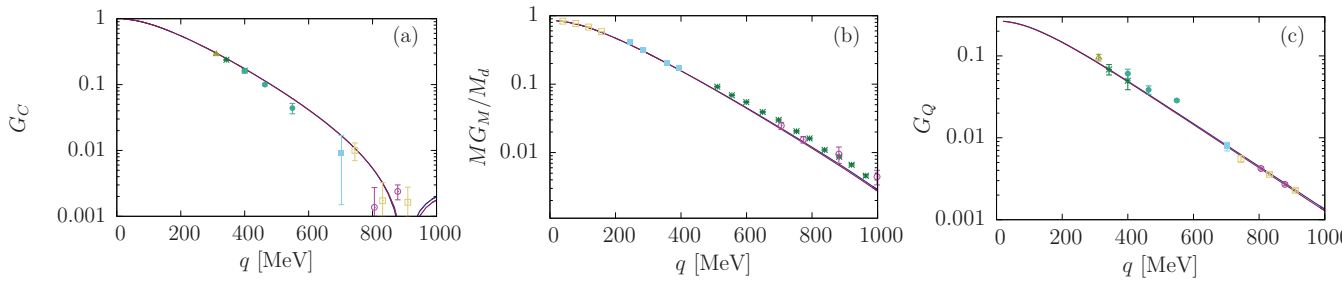

FIG. 2. (Color online) Deuteron form factors with theoretical error bands obtained by propagating the uncertainties of the $np + pp$ plus deuteron binding fit (see main text). Note that the theoretical error is so tiny that the width of the bands cannot be seen at the scale of the figure.

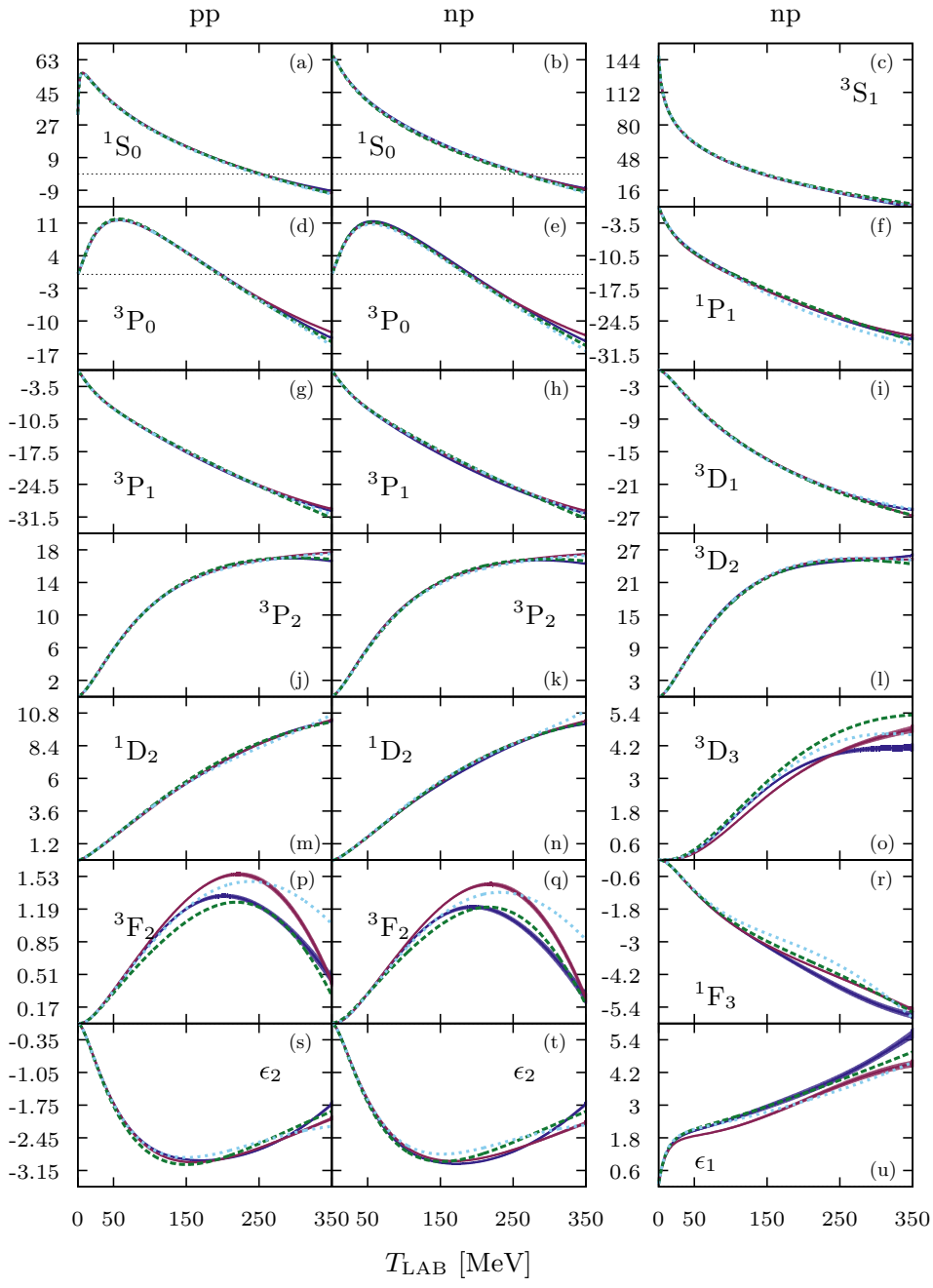

FIG. 3. (Color online) Lowest np and pp phase shifts (in degrees) and their errors (solid band) from the present χTPE analysis (red) and our previous OPE (blue). We also compare with the Nijmegen 1993 PWA [8] (light blue) and the AV18 [10] (green) as a function of the laboratory energy (in MeV).

TABLE VII. Deuteron static properties compared with empirical/recommended values and high-quality potential calculations. We list binding energy E_d, asymptotic D/S ratio η, asymptotic S-wave amplitude A_S, mean-squared matter radius r_m, quadrupole moment Q_D, D-wave probability P_D, and inverse matter radius $\langle r^{-1}\rangle$.

	This work	Emp./Rec. [36–41]	δ shell [15]	Nijm I [9]	Nijm II [9]	Reid93 [9]	AV18 [10]	CD-Bonn [11]
E_d (MeV)	Input	2.224575(9)	Input	Input	Input	Input	Input	Input
η	0.02473(4)	0.0256(5)	0.02493(8)	0.02534	0.02521	0.02514	0.0250	0.0256
A_S (fm$^{1/2}$)	0.8854(2)	0.8845(8)	0.8829(4)	0.8841	0.8845	0.8853	0.8850	0.8846
r_m (fm)	1.9689(4)	1.971(6)	1.9645(9)	1.9666	1.9675	1.9686	1.967	1.966
Q_D (fm^2)	0.2658(5)	0.2859(3)	0.2679(9)	0.2719	0.2707	0.2703	0.270	0.270
P_D	5.30(3)	5.67(4)	5.62(5)	5.664	5.635	5.699	5.76	4.85
$\langle r^{-1}\rangle$ (fm^{-1})	0.4542(2)		0.4540(5)		0.4502	0.4515		

two-body information (see, however, [25]), it opens up an interesting possibility regarding the inclusion of known isospin breaking effects at the OPE and TPE levels (see, e.g., [26] for a review). The small correction found in Ref. [27] requires an assumption on the regularization at short distances, which in our approach is equivalent to treating the $^1S_0$ channels for np and pp states as independent from each other.

The correlation ellipses for c_1, c_3, and c_4 are presented for 1σ, 2σ, and 3σ confidence levels in Fig. 1. The numerical values can be looked up in Table VI and compared to other determinations based on NN and πN information (see, e.g., Ref. [28] for many more πN determinations).

The PWA of the Nijmegen group with the same χTPE potential [13] but a different short-distance representation, included data up to $E_{\rm LAB} \leqslant 500$ MeV and gave $c_1 = -4.4(3.4)$ GeV^{-1} which is different from our findings that make it compatible with zero. We remind the reader that our NN analysis involves larger statistics (see Table IV) for $E_{\rm LAB} < 350$ MeV and hence the overall smaller uncertainties are not surprising. Similar to the Nijmegen group [13], we find a strong anticorrelation between c_1 and c_3. This allowed them to fix c_1 although the error estimate is based on taking the πN value for $c_1 = -0.76(7)$ GeV^{-1}. In our case, if we take $c_1 = -0.76$ GeV^{-1} as *input* we get after readjusting $c_3 = -4.42(7)$ GeV^{-1} and $c_4 = 4.47(16)$ GeV^{-1}, where again our errors are smaller presumably due to larger statistics for $E_{\rm LAB} < 350$ MeV.

The Nijmegen group found strong correlations of the chiral constants with the pion-nucleon coupling constant [13,14] when it is different from the recommended value $f^2 = 0.075$ [23,24]. This is the fixed value we took in both the selection of data in our previous work [15,16] as well as here. We chose not to change the coupling constant value, because this will have some impact on the data selection.

The recent values based on a χTPE fit up to $T_{\rm LAB} \leqslant 125$ MeV [29] are 2σ compatible with ours although no errors are reported, so it is unclear how many of the given digits are statistically significant. We find that lowering the energy range of the fit increases the uncertainties, making χTPE statistically irrelevant in that energy range (see also the discussion in Ref. [30] in connection to nuclear matrix elements). In Ref. [31] an error analysis of chiral constants from low-energy NN data and the deuteron using the N2LO χTPE based on a Monte Carlo, i.e., nonparametric, error propagation, was carried out revealing a branching structure in the three planes spanned by c_1, c_3, and c_4. It would be useful, though computationally costly, to carry out such error analysis in our scheme.

TABLE VIII. δ-shell potential parameters $V_{i,n}$ (in fm^{-1}) with their errors for all operators. We take $N = 3$ equidistant points with $\Delta r = 0.6$ fm. Rows marked with * indicates that the corresponding strength coefficients are not independent. In the first line we provide the central component of the δ shells corresponding to the EM effects below $r_c = 1.8$ fm. These parameters remain fixed within the fitting process.

Operator	$V_{1,x}$ $r_1 = 0.6$ fm	$V_{2,x}$ $r_2 = 1.2$ fm	$V_{3,x}$ $r_3 = 1.8$ fm
$V_C[pp]_{\rm EM}$	0.0072555	0.0065592	0.0016129
c	0.395(2)	−0.022(3)	−0.0119(9)
τ	0.030(2)	−0.036(1)	0.0025(2)
σ	−0.021(2)	0.041(1)	−0.0002(2)
$\sigma\tau$	−0.0410(8)	0.0417(7)	0.0021(1)
t	0.0	−0.002(2)	0.0008(2)
$t\tau$	0.0	0.1029(7)	0.0043(1)
ls	−0.1253(5)	−0.117(3)	0.0003(3)
$ls\tau$	−0.0418(2)	−0.025(1)	−0.0016(1)
$l2$	−0.2416(5)	0.022(3)	0.0005(2)
$l2\tau$	−0.0636(3)	−0.008(1)	0.00012(8)
$l2\sigma$	−0.0551(4)	0.000(1)	0.00003(9)
$l2\sigma\tau$	−0.0127(1)	−0.0027(4)	−0.00001(3)
$ls2$	0.1614(4)	0.030(5)	−0.0012(4)
$ls2\tau$	0.0538(1)	0.024(2)	−0.0010(1)
T	0.006(1)	−0.0003(2)	−0.00005(9)
σT^*	−0.006(1)	0.0003(2)	0.00005(9)
tT^*	0.0	0.0	0.0
τz^*	0.0	0.0	0.0
$\sigma\tau z^*$	0.0	0.0	0.0
$l2T^*$	−0.0010(2)	0.00004(4)	0.00001(1)
$l2\sigma T^*$	0.0010(2)	−0.00004(4)	−0.00001(1)

V. ERROR PROPAGATION

In Table VII we show our results for the deuteron static properties with their propagated errors and compared with our previous PWA and other high quality potentials. As we

TABLE IX. *pp* isovector phase shifts.

$E_{\rm LAB}$	$^1S_0$	$^1D_2$	$^1G_4$	$^3P_0$	$^3P_1$	$^3F_3$	$^3P_2$	ϵ_2	$^3F_2$	$^3F_4$	ϵ_4	$^3H_4$
1	32.654	0.001	0.000	0.133	−0.079	−0.000	0.014	−0.001	0.000	0.000	−0.000	0.000
	±0.003	±0.000	±0.000	±0.000	±0.000	±0.000	±0.000	±0.000	±0.000	±0.000	±0.000	±0.000
5	54.879	0.042	0.000	1.578	−0.886	−0.004	0.216	−0.051	0.002	0.000	−0.000	0.000
	±0.005	±0.000	±0.000	±0.002	±0.001	±0.000	±0.001	±0.000	±0.000	±0.000	±0.000	±0.000
10	55.313	0.165	0.003	3.726	−2.024	−0.031	0.652	−0.200	0.013	0.001	−0.003	0.000
	±0.007	±0.000	±0.000	±0.005	±0.002	±0.000	±0.002	±0.000	±0.000	±0.000	±0.000	±0.000
25	48.852	0.690	0.040	8.590	−4.837	−0.230	2.487	−0.806	0.106	0.021	−0.049	0.004
	±0.010	±0.001	±0.000	±0.016	±0.005	±0.000	±0.005	±0.000	±0.000	±0.000	±0.000	±0.000
50	39.176	1.679	0.154	11.532	−8.176	−0.690	5.840	−1.704	0.346	0.112	−0.196	0.026
	±0.015	±0.003	±0.000	±0.029	±0.009	±0.001	±0.008	±0.001	±0.001	±0.001	±0.000	±0.000
100	25.305	3.727	0.428	9.473	−13.161	−1.527	11.026	−2.684	0.857	0.478	−0.546	0.111
	±0.026	±0.007	±0.001	±0.041	±0.016	±0.005	±0.014	±0.005	±0.004	±0.003	±0.000	±0.000
150	15.179	5.636	0.709	4.665	−17.426	−2.143	14.037	−2.967	1.282	1.007	−0.863	0.222
	±0.038	±0.012	±0.002	±0.045	±0.022	±0.014	±0.018	±0.008	±0.009	±0.007	±0.000	±0.001
200	7.083	7.239	0.998	−0.384	−21.266	−2.582	15.719	−2.902	1.526	1.604	−1.128	0.347
	±0.053	±0.016	±0.004	±0.050	±0.032	±0.026	±0.021	±0.013	±0.017	±0.011	±0.001	±0.002
250	0.292	8.512	1.288	−5.029	−24.654	−2.845	16.696	−2.669	1.500	2.187	−1.345	0.483
	±0.071	±0.020	±0.008	±0.061	±0.048	±0.039	±0.028	±0.019	±0.026	±0.016	±0.002	±0.003
300	−5.563	9.504	1.567	−9.068	−27.515	−2.800	17.298	−2.363	1.144	2.689	−1.519	0.632
	±0.094	±0.030	±0.014	±0.078	±0.071	±0.046	±0.039	±0.028	±0.036	±0.024	±0.003	±0.005
350	−10.689	10.286	1.818	−12.438	−29.766	−1.907	17.682	−2.040	0.430	3.065	−1.653	0.794
	±0.120	±0.050	±0.023	±0.098	±0.098	±0.085	±0.050	±0.038	±0.045	±0.042	±0.004	±0.008

see there is a trend to produce smaller errors in the χTPE case as compared to the OPE result. The reason may be the slightly larger χ^2 value, which generically reduces the errors. The compatibility with our previous OPE study is at the 2σ level.

The deuteron form factors $G_C(Q)$, $G_M(Q)$, and $G_Q(Q)$ (see, e.g., [35] for a review) are depicted in Fig. 2 and come out with tiny error bands that cannot be distinguished within the plot scale from the ones obtained with OPE only in our previous work [15].

TABLE X. *np* isovector phase shifts.

$E_{\rm LAB}$	$^1S_0$	$^1D_2$	$^1G_4$	$^3P_0$	$^3P_1$	$^3F_3$	$^3P_2$	ϵ_2	$^3F_2$	$^3F_4$	ϵ_4	$^3H_4$
1	62.083	0.001	0.000	0.177	−0.106	−0.000	0.022	−0.001	0.000	0.000	−0.000	0.000
	±0.015	±0.000	±0.000	±0.000	±0.000	±0.000	±0.000	±0.000	±0.000	±0.000	±0.000	±0.000
5	63.652	0.041	0.000	1.617	−0.918	−0.004	0.255	−0.048	0.002	0.000	−0.000	0.000
	±0.038	±0.000	±0.000	±0.002	±0.001	±0.000	±0.001	±0.000	±0.000	±0.000	±0.000	±0.000
10	59.983	0.156	0.002	3.649	−2.021	−0.026	0.719	−0.182	0.011	0.001	−0.003	0.000
	±0.056	±0.000	±0.000	±0.006	±0.002	±0.000	±0.002	±0.000	±0.000	±0.000	±0.000	±0.000
25	50.895	0.672	0.033	8.197	−4.777	−0.198	2.590	−0.748	0.091	0.018	−0.039	0.003
	±0.091	±0.001	±0.000	±0.016	±0.005	±0.000	±0.005	±0.000	±0.000	±0.000	±0.000	±0.000
50	40.410	1.683	0.136	10.904	−8.122	−0.617	5.948	−1.619	0.310	0.101	−0.168	0.021
	±0.126	±0.003	±0.000	±0.029	±0.009	±0.001	±0.008	±0.001	±0.001	±0.001	±0.000	±0.000
100	26.350	3.787	0.402	8.750	−13.211	−1.410	11.076	−2.611	0.797	0.452	−0.495	0.095
	±0.160	±0.007	±0.001	±0.041	±0.016	±0.005	±0.014	±0.005	±0.004	±0.003	±0.000	±0.000
150	16.345	5.717	0.690	3.945	−17.588	−2.008	14.011	−2.930	1.204	0.970	−0.803	0.196
	±0.178	±0.013	±0.003	±0.046	±0.023	±0.014	±0.018	±0.009	±0.009	±0.007	±0.000	±0.001
200	8.437	7.306	0.991	−1.088	−21.525	−2.436	15.630	−2.904	1.430	1.559	−1.066	0.314
	±0.205	±0.017	±0.009	±0.051	±0.032	±0.027	±0.021	±0.013	±0.017	±0.011	±0.001	±0.002
250	1.858	8.541	1.298	−5.718	−24.988	−2.682	16.558	−2.707	1.384	2.132	−1.284	0.445
	±0.255	±0.020	±0.020	±0.062	±0.049	±0.039	±0.029	±0.020	±0.027	±0.016	±0.002	±0.003
300	−3.772	9.485	1.596	−9.742	−27.903	−2.581	17.125	−2.431	1.003	2.621	−1.461	0.589
	±0.328	±0.031	±0.037	±0.079	±0.072	±0.047	±0.040	±0.028	±0.036	±0.025	±0.003	±0.005
350	−8.658	10.218	1.868	−13.098	−30.187	−1.432	17.482	−2.130	0.261	2.982	−1.600	0.749
	±0.418	±0.052	±0.060	±0.100	±0.100	±0.114	±0.051	±0.039	±0.045	±0.043	±0.004	±0.008

TABLE XI. *np* isoscalar phase shifts.

$E_{\rm LAB}$	$^1P_1$	$^1F_3$	$^3D_2$	$^3G_4$	$^3S_1$	ϵ_1	$^3D_1$	$^3D_3$	ϵ_3	$^3G_3$
1	−0.189	−0.000	0.006	0.000	147.716	0.103	−0.005	0.000	0.000	−0.000
	±0.000	±0.000	±0.000	±0.000	±0.007	±0.000	±0.000	±0.000	±0.000	±0.000
5	−1.528	−0.010	0.217	0.001	118.103	0.641	−0.178	0.002	0.012	−0.000
	±0.002	±0.000	±0.000	±0.000	±0.015	±0.002	±0.000	±0.000	±0.000	±0.000
10	−3.148	−0.063	0.842	0.012	102.497	1.088	−0.665	0.004	0.079	−0.003
	±0.006	±0.000	±0.000	±0.000	±0.022	±0.005	±0.001	±0.000	±0.000	±0.000
25	−6.607	−0.421	3.689	0.170	80.418	1.634	−2.756	0.032	0.553	−0.053
	±0.018	±0.000	±0.003	±0.000	±0.034	±0.013	±0.004	±0.001	±0.000	±0.000
50	−10.086	−1.147	8.905	0.724	62.438	1.865	−6.344	0.254	1.613	−0.263
	±0.037	±0.001	±0.012	±0.000	±0.045	±0.024	±0.011	±0.006	±0.000	±0.000
100	−14.557	−2.310	17.147	2.200	42.803	2.161	−12.088	1.219	3.502	−0.971
	±0.067	±0.006	±0.039	±0.001	±0.053	±0.040	±0.024	±0.020	±0.003	±0.001
150	−18.070	−3.123	21.986	3.724	30.365	2.614	−16.318	2.348	4.842	−1.849
	±0.092	±0.013	±0.060	±0.004	±0.053	±0.053	±0.034	±0.035	±0.008	±0.003
200	−21.136	−3.756	24.371	5.166	21.054	3.166	−19.610	3.297	5.734	−2.765
	±0.121	±0.022	±0.071	±0.011	±0.055	±0.068	±0.039	±0.049	±0.016	±0.008
250	−23.794	−4.322	25.283	6.483	13.508	3.722	−22.324	3.988	6.304	−3.653
	±0.153	±0.036	±0.086	±0.025	±0.067	±0.085	±0.045	±0.067	±0.027	±0.017
300	−25.998	−4.891	25.404	7.644	7.100	4.196	−24.680	4.465	6.652	−4.485
	±0.186	±0.055	±0.116	±0.045	±0.091	±0.105	±0.063	±0.095	±0.039	±0.029
350	−27.677	−5.510	25.161	8.615	1.501	4.511	−26.802	4.808	6.852	−5.251
	±0.218	±0.080	±0.159	±0.072	±0.121	±0.124	±0.096	±0.131	±0.053	±0.045

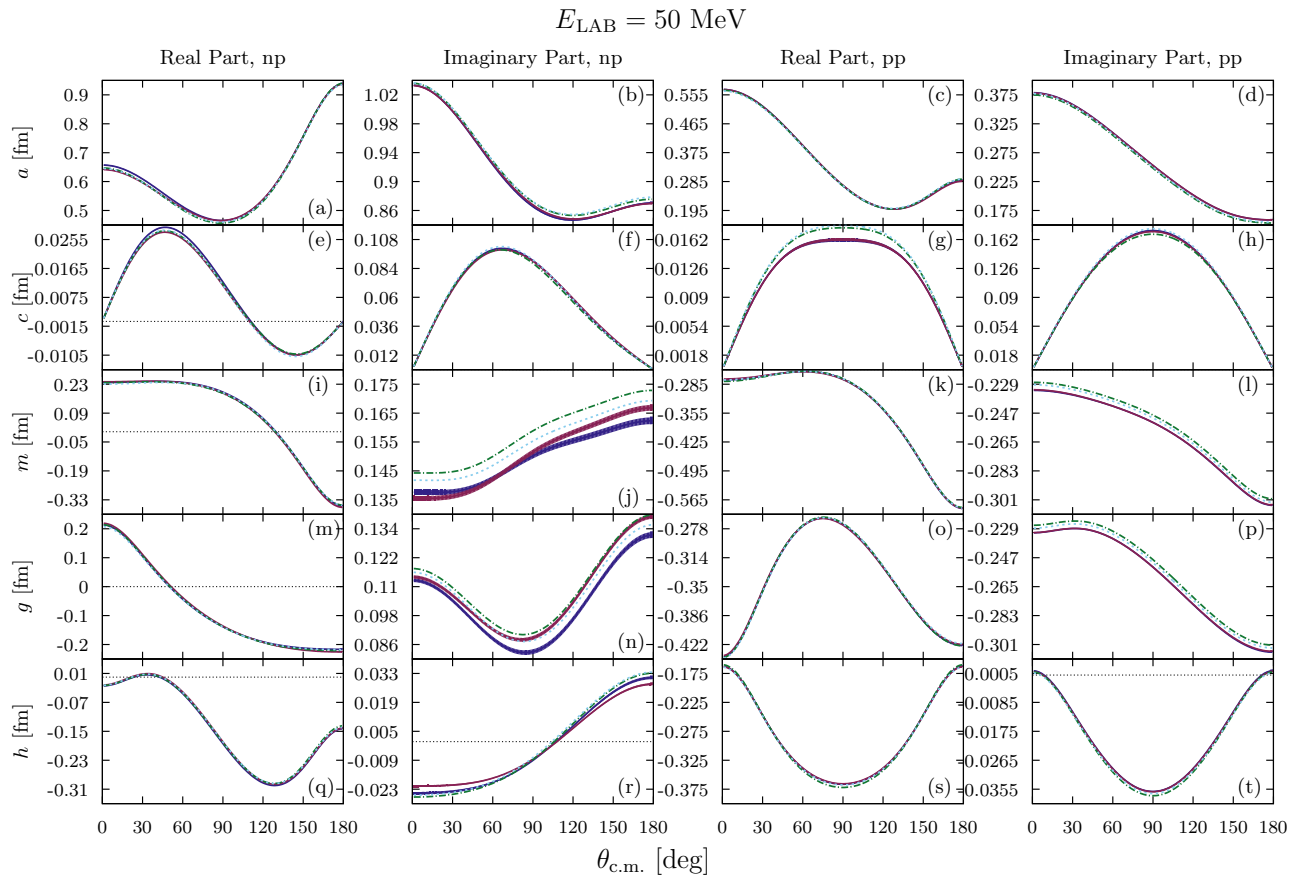

FIG. 4. (Color online) *np* (left) and *pp* (right) Wolfenstein parameters (in fm) as a function of the c.m. angle (in degrees) and for $E_{\rm LAB} = 50$ MeV. We compare our fit (blue band) with the PWA [8] (dotted, magenta) and the AV18 potential [10] (dashed-dotted, black) which provided a χ^2/d.o.f $\lesssim 1$ for data before 1993.

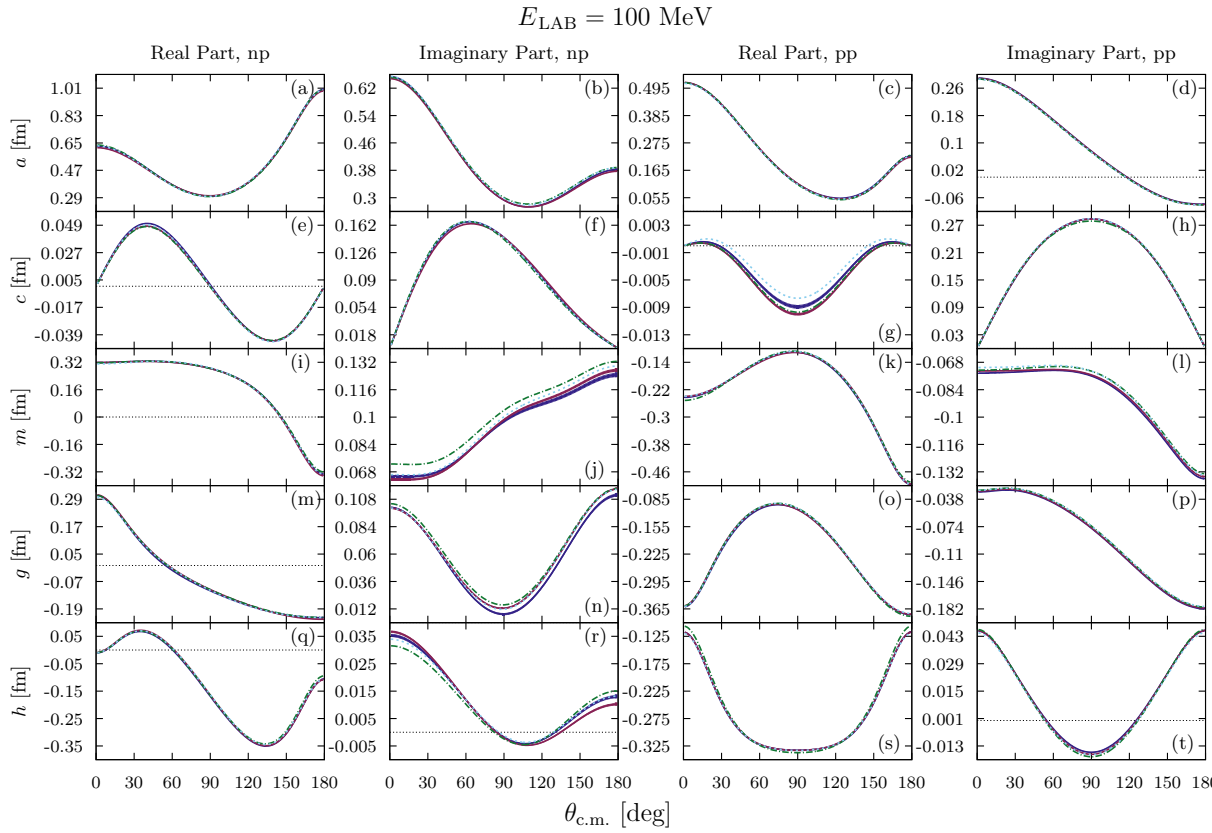

FIG. 5. (Color online) Same as in Fig. 4 but for $E_{\rm LAB} = 100$ MeV.

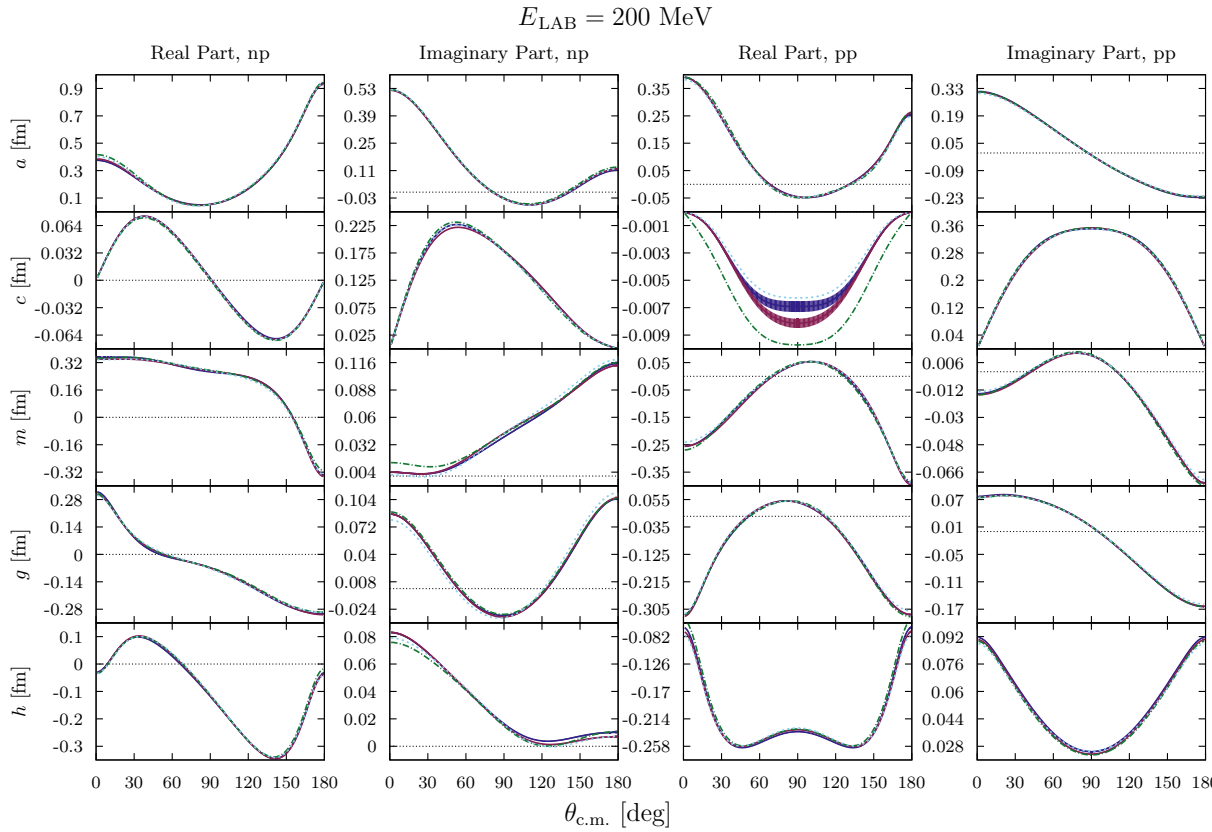

FIG. 6. (Color online) Same as in Fig. 4 but for $E_{\rm LAB} = 200$ MeV.

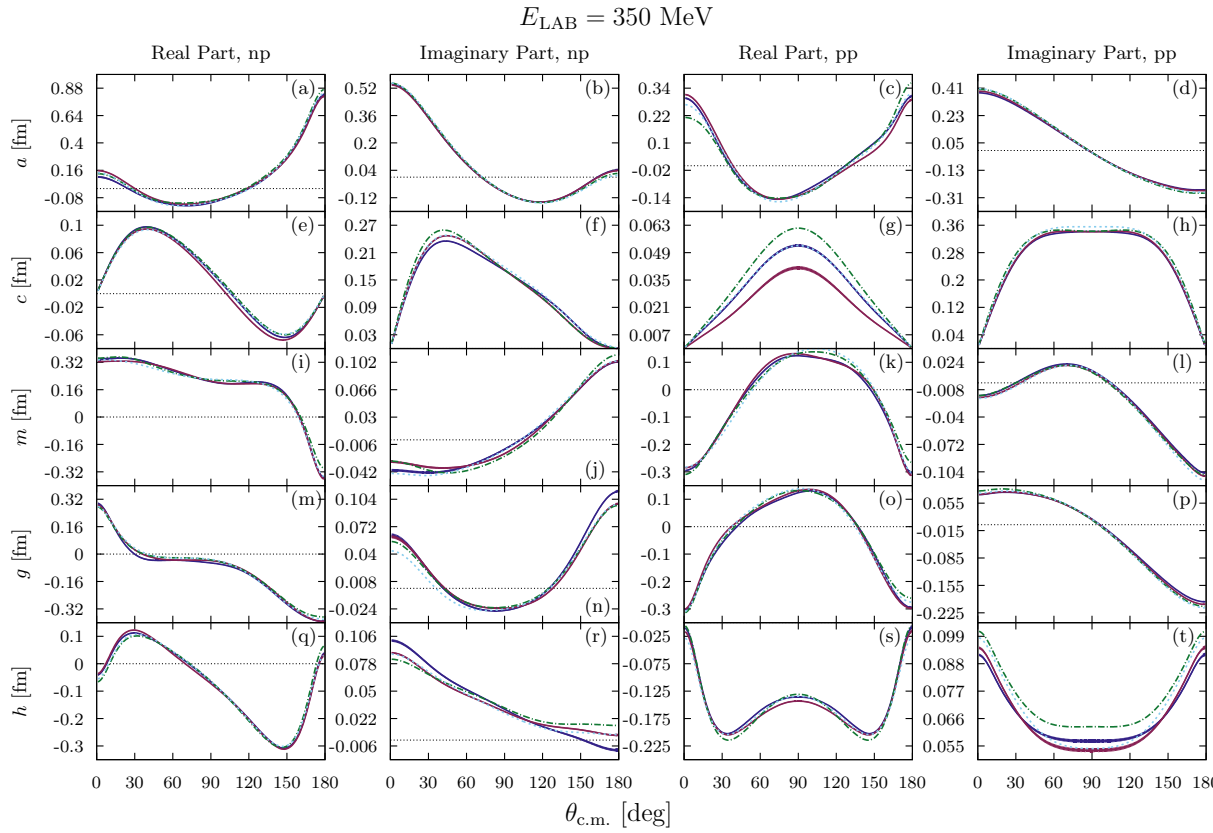

FIG. 7. (Color online) Same as in Fig. 4 but for $E_{\rm LAB} = 350$ MeV.

In Table VIII we show the strength operator coefficients $V_{i,n}$ [see Eq. (1)] and their statistical uncertainties propagated from the experimental data via the usual covariance matrix and applying the linear transformation to the partial wave short-distance parameters λ_i discussed in Ref. [15]. With these parameters and the covariance matrix it is possible to also estimate and propagate statistical error bars for calculations made with the δ-shell potential.

In Tables IX–XI we show pp isovector, np isovector, and np isoscalar phase shifts, respectively, with statistical errors extracted from experimental data for the lowest partial waves at different kinetic laboratory frame energy. A global overview can be appreciated in Fig. 3 where we plot these phases. For comparison we also draw the phase shifts from our previous OPE analysis [15,16], the Nijmegen PWA [8], and the AV18 potential [10]. As we see they agree within uncertainties for the lowest partial waves. Unfortunately the seminal Nijmegen group analysis of chiral potentials [13,14] did not provide phases, so a direct comparison which would reflect the effect of the different short-distance parametrizations cannot be made. The discrepancies apparent in higher partial waves among *all potentials* take place also in the scattering amplitude as shown in Figs. 4–7 and suggest the presence of some small systematic errors. The systematic vs statistical error dominance was already noted in Refs. [20,34]. A nonparametric statistical analysis along the lines pursued in Ref. [31] for the complete database might possibly shed light onto this issue and is left for future research.

VI. CONCLUSION

We summarize our points. The chiral constants c_1, c_3, and c_4 characterizing the χTPE potential at N2LO have been determined with errors by analyzing *NN* scattering data published from 1950 to 2013 below 350 MeV with a $\chi^2/\nu = 1.08$. The values found are in the bulk of other determinations, although our higher data statistics allows us to reduce previous error estimates based on *NN* scattering data and the deuteron. At the same time we provide quantitative error estimates of the short-distance component of the interaction hence allowing error propagation of the much used χTPE interactions in nuclear structure calculations. We have also provided extensive tables of phase shifts with uncertainties based on the present analysis. The verification and control of errors in the *NN* interaction is an important test to check the validity and statistical reliability of theoretical predictions with a prescribed confidence level. Our results suggest that chiral interactions may play an important role in nuclear structure calculations within the errors inherited from the existing *NN* data.

ACKNOWLEDGMENTS

This work was supported by Spanish DGI (Grant No. FIS2011-24149) and Junta de Andalucía (Grant No. FQM225). R.N.P. is supported by a Mexican CONACYT grant.

[1] S. Weinberg, Phys. Lett. B **251**, 288 (1990).
[2] C. Ordonez and U. van Kolck, Phys. Lett. B **291**, 459 (1992).
[3] C. Ordonez, L. Ray, and U. van Kolck, Phys. Rev. C **53**, 2086 (1996).
[4] E. Epelbaum, H.-W. Hammer, and U.-G. Meissner, Rev. Mod. Phys. **81**, 1773 (2009).
[5] R. Machleidt and D. Entem, Phys. Rep. **503**, 1 (2011).
[6] N. Kaiser, R. Brockmann, and W. Weise, Nucl. Phys. A **625**, 758 (1997).
[7] E. Epelbaum, Prog. Part. Nucl. Phys. **57**, 654 (2006).
[8] V. G. J. Stoks, R. A. M. Klomp, M. C. M. Rentmeester, and J. J. de Swart, Phys. Rev. C **48**, 792 (1993).
[9] V. G. J. Stoks, R. A. M. Klomp, C. P. F. Terheggen, and J. J. de Swart, Phys. Rev. C **49**, 2950 (1994).
[10] R. B. Wiringa, V. G. J. Stoks, and R. Schiavilla, Phys. Rev. C **51**, 38 (1995).
[11] R. Machleidt, Phys. Rev. C **63**, 024001 (2001).
[12] F. Gross and A. Stadler, Phys. Rev. C **78**, 014005 (2008).
[13] M. C. M. Rentmeester, R. G. E. Timmermans, J. L. Friar, and J. J. de Swart, Phys. Rev. Lett. **82**, 4992 (1999).
[14] M. C. M. Rentmeester, R. G. E. Timmermans, and J. J. de Swart, Phys. Rev. C **67**, 044001 (2003).
[15] R. Navarro Pérez, J. E. Amaro, and E. Ruiz Arriola, Phys. Rev. C **88**, 024002 (2013).
[16] R. N. Perez, J. E. Amaro, and E. R. Arriola Phys. Rev. C **88**, 064002 (2013).
[17] J. B. Aviles, Phys. Rev. C **6**, 1467 (1972).
[18] D. R. Entem, E. Ruiz Arriola, M. Pavon Valderrama, and R. Machleidt, Phys. Rev. C **77**, 044006 (2008).
[19] R. Navarro Perez, J. Amaro, and E. Ruiz Arriola, Prog. Part. Nucl. Phys. **67**, 359 (2012).
[20] R. Navarro Perez, J. Amaro, and E. Ruiz Arriola, Phys. Lett. B **724**, 138 (2013).
[21] R. Navarro Perez, J. E. Amaro, and E. Ruiz Arriola, PoS **CD12**, 104 (2013), arXiv:1301.6949.
[22] R. Navarro Pérez, J. E. Amaro, and E. Ruiz Arriola, Few-Body Syst. (2014), doi:10.1007/s00601-014-0817-3.
[23] V. G. J. Stoks, R. Timmermans, and J. J. de Swart, Phys. Rev. C **47**, 512 (1993).
[24] J. J. de Swart, M. C. M. Rentmeester, and R. G. E. Timmermans, PiN Newslett. **13**, 96 (1997).
[25] A. Calle Cordon, M. Pavon Valderrama, and E. Ruiz Arriola, Phys. Rev. C **85**, 024002 (2012).
[26] G. A. Miller, A. K. Opper, and E. J. Stephenson, Ann. Rev. Nucl. Part. Sci. **56**, 253 (2006).
[27] U. van Kolck, M. C. M. Rentmeester, J. L. Friar, T. Goldman, and J. J. de Swart, Phys. Rev. Lett. **80**, 4386 (1998).
[28] J. Alarcon, J. Martin Camalich, and J. Oller, Ann. Phys. (NY) **336**, 413 (2013).
[29] A. Ekström, G. Baardsen, C. Forssén, G. Hagen, M. Hjorth-Jensen *et al*., Phys. Rev. Lett. **110**, 192502 (2013).
[30] J. E. Amaro, R. Navarro Pérez, and E. Ruiz Arriola, Few-Body Syst. (2013), doi:10.1007/s00601-013-0756-4.
[31] M. Pavon Valderrama and E. Ruiz Arriola, Phys. Rev. C **74**, 054001 (2006).
[32] D. R. Entem and R. Machleidt, Phys. Rev. C **68**, 041001 (2003).
[33] P. Buettiker and U.-G. Meissner, Nucl. Phys. A **668**, 97 (2000).
[34] R. Navarro Perez, J. E. Amaro, and E. Ruiz Arriola, arXiv:1202.6624.
[35] R. A. Gilman and F. Gross, J. Phys. G **28**, R37 (2002).
[36] C. V. D. Leun and C. Alderliesten, Nucl. Phys. A **380**, 261 (1982).
[37] I. Borbly, W. Grebler, V. Knig, P. A. Schmelzbach, and A. M. Mukhamedzhanov, Phys. Lett. B **160**, 17 (1985).
[38] N. L. Rodning and L. D. Knutson, Phys. Rev. C **41**, 898 (1990).
[39] S. Klarsfeld, J. Martorell, J. A. Oteo, M. Nishimura, and D. W. L. Sprung, Nucl. Phys. A **456**, 373 (1986).
[40] D. M. Bishop and L. M. Cheung, Phys. Rev. A **20**, 381 (1979).
[41] J. J. de Swart, C. P. F. Terheggen, and V. G. J. Stoks, arXiv:nucl-th/9509032.